

**Lightning observations of a small satellite “Maido-1”
and the study on recorded VHF waveforms**

Takeshi Morimoto¹, Hiroshi Kikuchi², Satoru Yoshida³, Tomoo Ushio²
and Zen-Ichiro Kawasaki²
Maido-1 Satellite Project Team

¹ Kindai University, 3-4-1 Kowakae, Higashiosaka City, Osaka 577-8502, Japan
E-mail: morimoto@ele.kindai.ac.jp

² Osaka University, 2-1 Yamadaoka, Suita, Osaka 565-0871, Japan

³ Meteorological Research Institute, 1-1 Nagamine, Tsukuba 305-0052, Japan.

Abstract. This paper reviews developments and lightning observations on a small satellite “Maido-1” and its electromagnetic (EM) payload, the very high frequency (VHF) sensor. Maido-1 satellite was launched on January 23, 2009 and injected into the sun-synchronous polar orbit at an altitude of 660 km. A radio frequency receiver was installed on Maido-1 to examine the feasibility of the space-based digital interferometer receiving lightning EM impulses in VHF band. Through the nine months of the operation period of Maido-1, the VHF sensor conducted 158 lightning observations and recorded about 15,000 VHF EM waveforms around the world. The main achievements of the VHF sensor on Maido-1 are 1) functional confirmation of the sensor manufactured by commercial off-the-shelf products, 2) validation of the sensor sensitivity designed by the numerical estimation for the attenuation in the propagation path, and 3) verification of the available EM noise environment for the lightning observation on the orbit. Characteristics of pulse duration and pulse pair founded in the recoded waveforms are studied using numerical simulation for a layered ionosphere model. This paper also proposes the estimation considering the ionospheric propagation, and its effectiveness is demonstrated.

Key words: lightning observations, radio propagation, VHF broadband electromagnetic wave, small satellite, ionosphere

1. Introduction

Maido-1 satellite project represents a technology transfer program to expand the range of the space development community in Japan (Kato et al. 2005; Nakamura and Hashimoto 2004, 2005; Okubo and Azuma 2006). From the late years of 20th century small satellites and those research and development (R&D) are highly focused expecting to pave the way which is a faster, cheaper, and better for space utilization. Space Technology Demonstration Research Center of Japan Aerospace Exploration Agency (JAXA) had developed and was launched their own first small satellite, “MicroLabSat” in December, 2002 (Nakamura et al. 2003, Ohtsubo et al. 2003). A group of small and medium-sized

enterprises (SMEs) and factories in Kansai region established the Space Oriented Higashiosaka Leading Association (SHOLA) in 2003. Under the cooperative agreement, JAXA intends to contribute to socio-economic development by returning its R&D results to society; meanwhile, SOHLA tries to revitalize the local economy through the commercialization of versatile small satellites. According to the agreement, JAXA discloses the technical information related to small satellites and provides technical support so that SOHLA and collaborative universities can acquire fundamental space technologies through system management and satellite design, manufacturing, testing, and operation of Maido-1.

The authors proposed the lightning observations as a scientific mission and joined the Maido-1 satellite project. We have developed the ground-based very high frequency (VHF) broadband Digital InTerFerometer (DITF) to image precise lightning channels and to monitor lightning activities. The remarkable feature of DITF is its ultra-wide bandwidth (from 25 to 100 MHz) and implicit redundancy for estimating VHF source locations (Mardiana et al. 2000; Morimoto et al. 2004). The VHF sensor on Maido-1 satellite is the first step in our gradual approach to realize space-borne DITF (Morimoto et al. 2011). The VHF sensor comprises a system to record VHF broadband electromagnetic (EM) signals. It examines the feasibility of the space-borne DITF receiving VHF lightning impulses in space. Maido-1 satellite was launched successfully and has been operated for nine months in 2009. This paper describes the development of Maido-1 satellite and its payload, the VHF sensor. It also discussed the recorded VHF waveforms.

2. Maido-1 satellite

Maido-1 is a spin-stabilized microsatellite based on MicroLabSat heritage with the weight of about 50 kg as shown in Fig. 1. It is an octagonal prism having two deployable booms and VHF rod type antenna. The spin axis is fixed to the inertial reference frame which lies in the plane containing the solar direction and the normal to the orbital plane. The prime objective of the Maido-1 satellite project is to achieve a low-cost and short term development of a microsatellite which utilizes the components and bus technologies of JAXA's MicroLabSat. The major specifications and the architecture of Maido-1 are shown in Table 1 and Fig. 2, respectively. All the attitude control system (ACS), the communication system (COM), the electric power system (EPS), and the experimental systems are connected to the satellite's main central and data handling (DH) system called central control unit (CCU) and extended control unit (ECU). The spin control and nutation damping are implemented by driving magnetic torques (MTQ) with

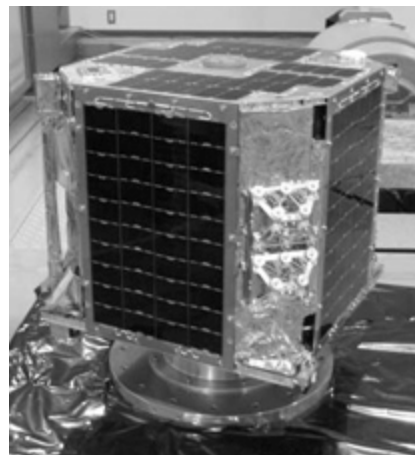


Figure 1. External appearance of Maido-1.

Table 1. Specifications of Maid-1.

Weight	57 kg
Size	500 mm × 500 mm × 500 mm Octagonal prism and two deployable booms
Power	~70 W
Attitude control system (ACS)	Spin stabilized (3 rpm nominal) with magnetic torquers for spin axis control
Thermal control subsystem	Passive implementation
Electric power system (EPS)	- 30 ~ 40 W of power, face-mounted GaAs solar cells - Ni-MH battery, 34 V - Peak power tracking control
RF communications	- Single S-band 4096 bps downlink / 500 bps uplink - Amateur band (VHF) downlink
Navigation	Single frequency GPS system (L1)
Orbit	Sun-synchronous near-circular orbit Altitude: 666 km, Inclination: 98.06°

onboard computing. The spin axis is estimated using solar sensors (CSS) and magnetic sensors (FMS), and it is controlled based on offline computing.

The concept of the satellite was simple and low cost. Therefore the satellite was designed and manufactured by applying as many MicroLabSat technologies as possible, SMEs' low cost manufacturing techniques, and a redundant and fail-safe configurations to the critical components of the system. The Nickel-Metal Hydride (Ni-MH) battery (BAT), S-band transponder/diplexer (SDIP) and coupler (SCPL)/antenna were adopted the same components as MicroLabSat.

The component design of CCU, ECU and Power Control Units (PCU), the system technology of the peak power tracking control algorithm, the spin-axis control algorithm, the system design and development software, and the S-band operation system were transferred from MicroLabSat. Aluminum isogrid panels were used instead of conventional honeycomb panels in the main structure of the

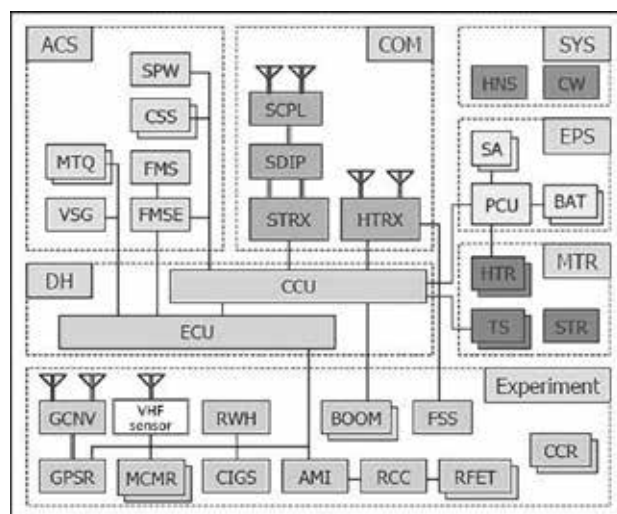


Figure 2. System architecture of Maido-1.

satellite in order to reduce the weight and manufacturing costs. Isogrid panels are also effective as radiation shields for facilitating the use of commercial off-the-shelf (COTS) parts. A redundant and fail-safe configuration to the critical components of the system was applied. COM combines amateur band (HTRX) and S-band transceiver/receiver (STRX). Solar cells (SA) were mounted on every panel to provide the minimum survival power even in a case of attitude loss. If the satellite is not operated for the set predetermined time, it goes into the survival mode in which only main missions and collections of necessary telemetry are continued.

Maido-1 had additional seven technology demonstration experiments besides the VHF sensor;

- Orbit determination technology experiment and its component demonstration
- Space-environment measurement experiment and its component demonstration
- Demonstration of copper indium gallium selenide (CIGS) solar cells experiment
- Demonstration of space-qualified 200 MIPS 64-bit microprocessor: Advanced Microprocessing In-orbit experiment (AMI)
- Small monitor camera (MCMR) demonstration
- Deployable boom demonstration (BOOM)
- Demonstration of a students’ sun sensor (FSS) and sun angle calculation algorithm

Maido-1 was launched on January 23, 2009 on the H-IIA rocket as a secondary payload on the GOSAT primary mission, and injected into the sun-synchronous near-circular orbit with an altitude of 666 km and an inclination of 98.06°. The satellite operation/control and the data download with the primary S-band communications link were conducted at the JAXA Space Technology Demonstration Research Center being supported by the ground station network of JAXA, Masuda, Okinawa and Katsuura stations. The nominal operation phase had been carried out under a good condition for three months (March – May 2009), and subsequently followed by the extended operation phase (June – September 2009) (Okubo *et al.* 2009). In the operation period, all components were working well and obtaining the data successfully. The mission was terminated on October 15, 2009 by the command from the ground station after all mission objectives had been completed satisfactorily.

3. VHF sensor

Figure 3 shows the configuration diagram of the VHF sensor. The sensor comprises a single set of an antenna, a band-pass filter, an amplifier and an analog-to-digital (AD) converter. The antenna is rod-type with a length of 1 m and made of a convex shape spring steel. It is rolled and tied with gut in launching, and the antenna is extended by cutting the gut in the orbit. Figure 4 is an actual photograph of Maido-1 which was taken in the EM test for the VHF sensor with the antenna extension. As the spin axis of the satellite is perpendicular to the antenna, the antenna rotates parallel to the Earth’s surface. The band-pass filter has a 3 dB pass band from 30 to 100 MHz with 20 dB

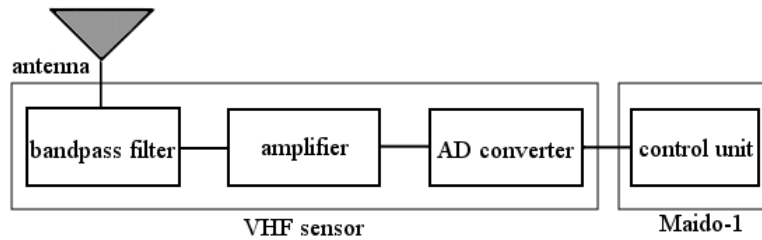


Figure 3. Configuration diagram of the VHF sensor.

attenuation at 20 and 110 MHz. The gain of the amplifier is designed to be 45 dB. In the case of the ground-based DITF, with an observation range of around a hundred kilometers, the dynamic range is given more importance than the gain. A space-borne system, on the other hand, requires high gain because the intensities of received EM signals are inversely proportional to the distance between the EM radiation source and the receiving antenna. The gain of the amplifier is determined to be 45 dB, adding 20 dB to the ground-based DITF on the pretext of numerical estimation for attenuation in the propagation path (Taniguchi et al. 2006). The AD converter has a sampling rate of 200 MS/s and 8-bit resolution to record VHF broadband EM signals. It is known that thousands of impulsive VHF EM pulses are radiated intermittently in association with lightning leader development. The typical pulse width of each radiation is hundreds nanoseconds. Therefore the AD converter is designed to record the waveforms with a duration of 2.5 μ s by the event triggering sequence. It means that a waveform for 2.5 μ s is recorded with 50% of pre-triggering when input signal exceeds the threshold voltage. The maximum number of waveforms as one dataset is 100 due to the size of the onboard memory of the AD converter. The AD converter is connected to the control unit (ECU) of the satellite with

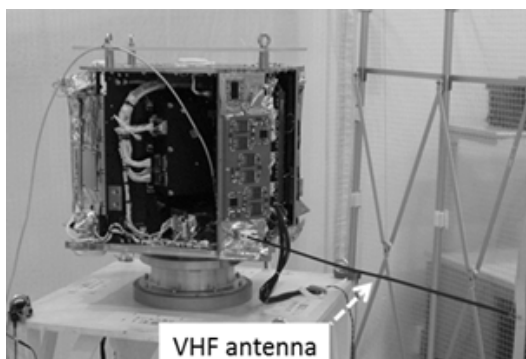


Figure 4. VHF antenna on Mado-1 without side solar panels. The antenna is extended on the orbit.

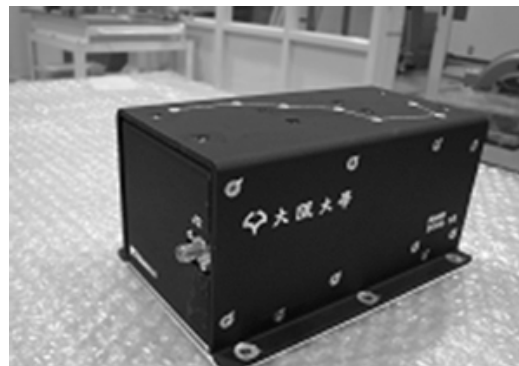


Figure 5. VHF sensor electronics unit.

Table 2. Specifications of the VHF sensor.

Outline	
Weight	950 g
Size	100 mm × 80 mm × 150 mm
Power	4 W (5 V: 1.8 W, 15 V: 2.2 W)
Communications interface	19200 bps RS-422
Band-pass filter	
3 dB pass band	30 ~ 100 MHz
Insertion loss	-1 dB (at center frequency)
Attenuation	-20 dB at 20 and 110 MHz
Input and output impedance	50 Ω
Amplifier	
Input level	-85 ~ -35 dBm
Gain	45 dB
Output level	1 V _{p-p}
Input and output impedance	50 Ω
AD converter	
Data sampling speed	200 MS/s
AD resolution	8 bit
Input channel	1 channel
Input impedance	50 Ω
Coupling	AC
Input level	1 V _{p-p}
Input frequency	20 ~ 100 MHz
Triggering	Level trigger (event trigger)
Threshold level	50 ~ 500 mV (10 steps variable, positive only)
Memory	Ring-buffer for 100 × 2.5 μsec waveforms

RS-422 interface. The AD converter is controlled by the commands from ECU and the captured data are transferred through ECU. The VHF sensor is not an interferometer, but just a VHF EM recorder to examine the feasibility of the space-borne DITF.

The VHF sensor was developed based on the components of the ground-based DITF. Some critical parts were replaced with resistant ones to radiation, vacuum and thermal environment in the orbit. Some modifications were implemented as countermeasures against vibration in launching and heat conduction in vacuum. The VHF sensor with a lot of COTS parts are validated by repeated environmental tests such as vibration and thermal vacuum tests. The electronics unit of the VHF sensor except for the antenna and the specifications are shown in Fig. 5 and Table 2, respectively.

4. Results and discussion

4.1. Overview

The VHF sensor conducted 158 sets of EM observations during the nominal and extended operation periods from February to October 2009. Through the observations, the VHF sensor recorded 14,372 waveforms, and 1013 waveforms in 116 datasets of them were downloaded to the ground station. Figure 6 shows the locations where the VHF sensor was turned on. Most observations were conducted at areas where active lightning was expected by weather forecast. Squares, triangles and crosses in Fig. 6 represent the number of recorded VHF waveforms, i.e. the number of triggering, at each observation for several seconds; \diamond : less than 50, \triangle : less than 100, and $+$:100 triggerings. A bunch of lineal plots were obtained by successive observations in one satellite path. Clear contrast of active (+) and non-active (\diamond) VHF radiations are noticeable between over land and sea. They agree with the past investigations by the optical observations (Boccippio et al. 2000; Christian et al. 2003). Even over ocean, significant numbers of VHF signals were recorded above the Atlantic Ocean, as shown in Fig.6. This point is discussed in the next section.

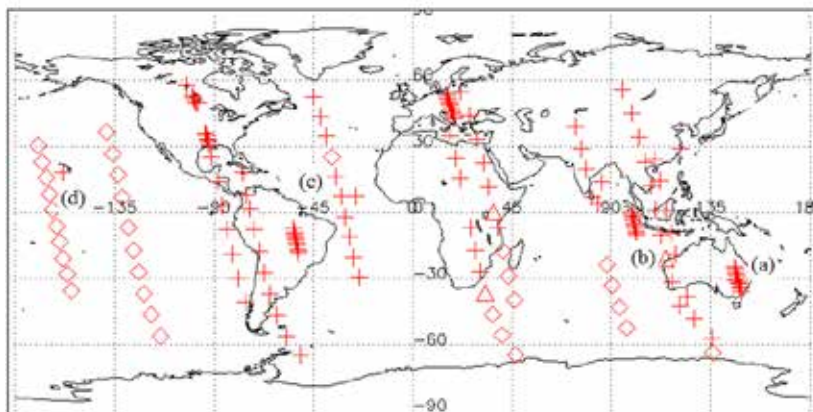


Figure 6. Locations of the VHF sensor observations.

4.2. Regional dependence

Figure 7 shows the typical waveforms captured at four different areas, (a) Eastern Australia, (b) Southeast Asia, (c) Atlantic Ocean, and (d) Pacific as written in Fig. 6. The waveforms in Fig. 7d were recorded above the Pacific Ocean where is a non-lightning activity area by the forced triggering. From the comparison of the waveforms in Fig. 7, the intensity of EM signal is small enough when there is no lightning activity (Fig. 7d). On the other hand, the variations of the intensity are identified caused by lightning discharges at an altitude of 660 km (Fig. 7abc). These results indicate that VHF broadband EM signals are applicable for the lightning observation from the orbit. In other words, the EM background at the orbit is appropriate for VHF observations. Since the waveforms in Fig. 7 are drawn in the full ranges of the receiver, the adequacy of the designed sensitivity can be validated as well.

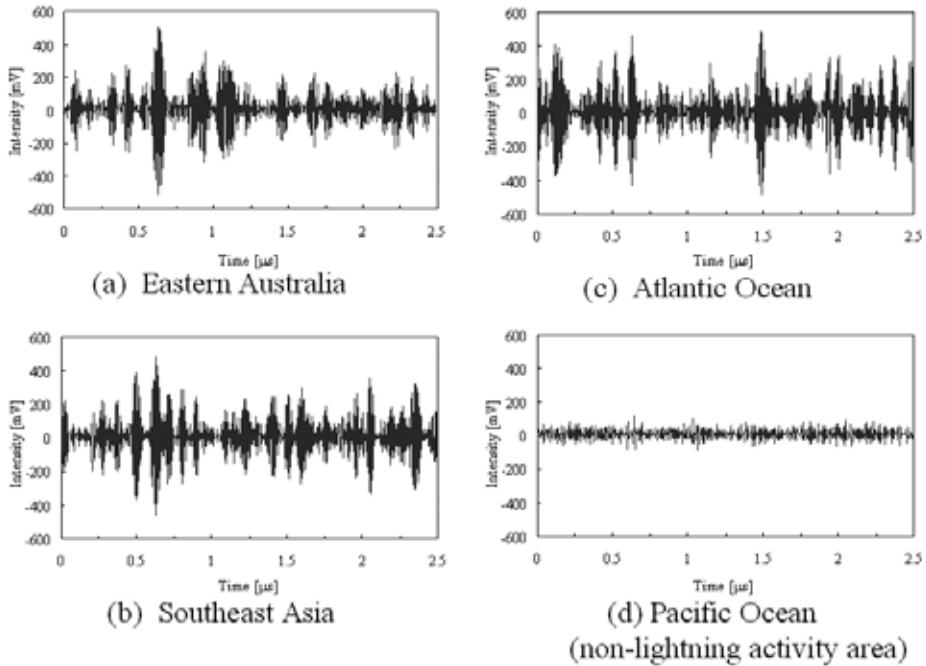


Figure 7. Typical waveforms recorded by the VHF sensor.

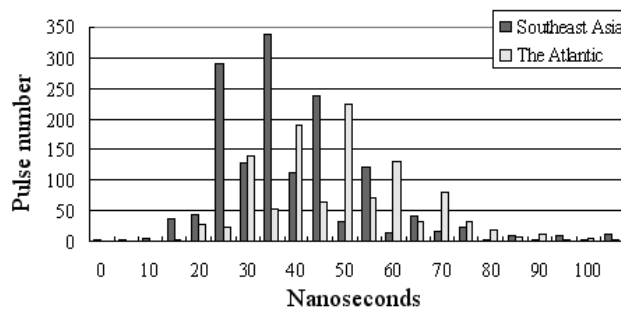


Figure 8. Frequency distribution of FWHMs recorded by the VHF sensor at Southeast Asia and the Atlantic.

Figure 8 shows the frequency distribution of the full width at half maximum (FWHM) for 1528 and 630 pulses recorded at Southeast Asia and the Atlantic, respectively. Several pulses were counted in one waveform for 2.5 μs , if detectable. From the Fig. 8, it is noticed that the FWHM of the pulses at the Atlantic is about 20 ns longer than the pulses at Southeast Asia. Considering the dispersion of the ionosphere, the farther EM source corresponds to the wider FWHM as simulated in the next section. The results in Fig. 8 can be explained that the pulses recorded at the Atlantic are radiated from lightning discharges on Africa with diagonal long propagation path in the ionosphere.

4.3. Simulation of EM propagation in the ionosphere

Waveforms of the VHF sensor are received after the ionospheric propagation under the satellite orbit at an altitude of 660 km. Since the ionosphere is a dispersive medium, the effect to the waveform has frequency dependence. The change in waveform propagating inside the ionosphere is simulated in this section.

Assume that the ionosphere as a spherical layer structure in which the charge density varies by a thickness of 10 km. In this model, the index of refraction is constant in a layer of 10 km and it differs from one layer to another. The refraction index n is expressed as (Kikuchi et al. 2011; Taniguchi et al. 2006)

$$n = \sqrt{1 - f_p^2 / f^2} \dots\dots\dots (1)$$

Here, f_p and f are plasma frequency and propagating EM frequency, respectively. The plasma frequency f_p is given by

$$f_p = \frac{1}{2\pi} \sqrt{\frac{Ne^2}{m\epsilon_0}} \dots\dots\dots (2)$$

Substituting the electron mass m and the permittivity of free space ϵ_0 into the Eq. (2), f_p can be approximated as

$$f_p \approx 8.89\sqrt{N} \dots\dots\dots (3)$$

using the charge density N . In our simulation, N at each altitude is given from the international reference ionosphere (IRI) model (IRI database 2007). The altitude of the bottom of the ionosphere is 80 km according to the IRI model. The propagation path is simulated for a certain incident angle θ_0 to the bottom layer applying the Snell’s law at every boundary as illustrated in Fig. 9. Using the above model the lengths of the ionospheric propagation path from the bottom altitude ($R_0 = 80$ km) to the satellite altitude (660 km) are calculated for various frequencies. In lower frequency, the length becomes longer which is caused by the larger refraction than in higher frequencies. As a result, the lower frequency components delay, i.e. group delay, and the pulse duration is expanded. The simulated VHF pulse waveforms at various altitudes are shown in Fig. 10 (Taniguchi et al. 2006). The original waveform is a modulated Gaussian pulse with a frequency bandwidth between 30 and 100 MHz and a pulse duration of 200 ns. The simulated waveforms are obtained by the inverse Fourier transform after taking into account the phase differences based on the calculated group delay. The simulated waveforms in Fig. 10 correspond to an angle of incidence of 30° and a distribution of charge

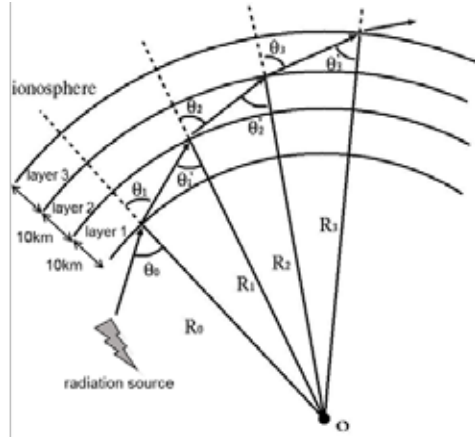


Figure 9. Simulation model of the ionosphere with spherical layers.

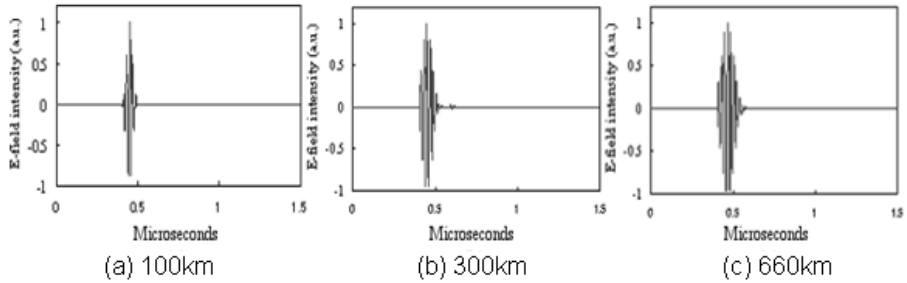


Figure 10. Numerical simulation of altitude variation of a VHF waveform.

density in nighttime. The long pulse duration with large dispersion effect at a high altitude is represented. The simulated pulse duration and the EM radiation source are compared in Kikuchi *et al.* (2011) referring to the World Wide Lightning Location Network (WWLLN) data.

4.4. Pulse pair

Pulse pairs as shown in Fig. 11 are recognized in 20% and 10% of recorded pulse at Southeast Asia and Africa, respectively. The features common to these pulse pairs are;

- Amplitude and duration are similar among pulse pairs.
- Time separation between pulse pairs ranges from 40 to 1000 ns.
- Amplitudes of pulse pairs are relatively weak in recorded EM pulses.

These pulse pairs are decidedly different from the transionospheric pulse pair (TIPP) reported in the past satellite observations (Tierney *et al.* 2002) in terms of the time separation. We infer the cause of them as the mode splitting that is difference of EM propagation in the ordinary (O) and the extra ordinary (X) modes. The simulation model in the previous section is expanded its application taking the geomagnetic effect into account to confirm the inference. Referring to the Appleton-Hartree equation (Sen and Wyller 1960), the refraction index of this model is given by

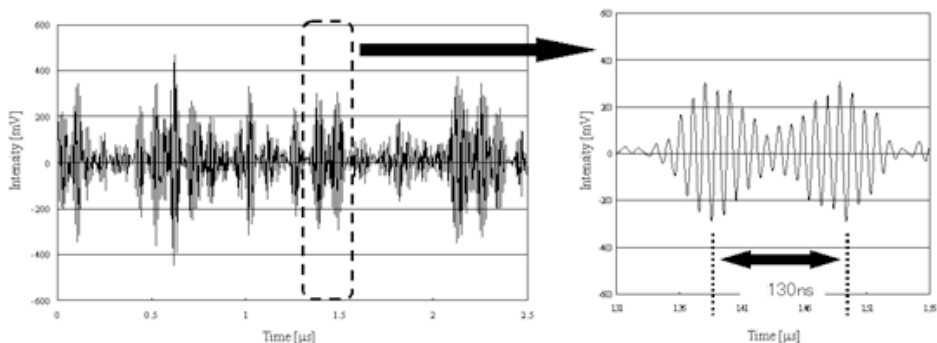


Figure 11. Pulse pair observed by the VHF sensor.

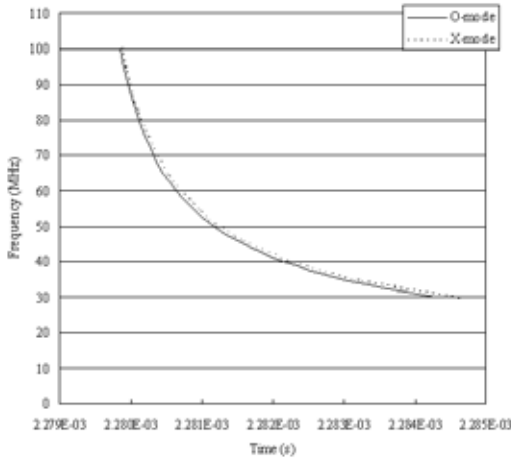


Figure 12. Simulated propagation time of O and X modes.

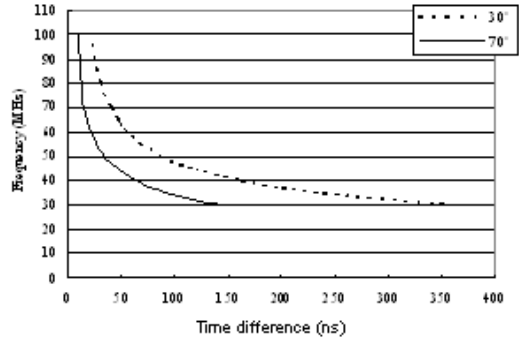


Figure 13. Simulated propagation time difference between O and X modes.

$$n = \sqrt{1 - \frac{X}{1 \pm Y \cos \theta}}, \quad (X = f_p^2 / f^2, Y = f_H / f)$$

..... (4)

where f_p and f_H is the plasma and the cyclotron frequencies, respectively. The angle between the vectors of geomagnetism and EM propagation is represented as θ . The geomagnetism of the international geomagnetic reference field (IGRF) model (IGRF-10 database 2009) is used in the simulation. The pulse and minus signs in the right side of Eq. (4) correspond to the O and X modes, respectively (Kikuchi et al. 2010a, 2010b). The received waveform is simulated by the similar method to the previous section but using Eq. (4) instead of Eq. (1). The propagation times of two modes from an altitude of 80 km to 660 km with an incident angle of 30° is graphed in Fig. 12. The propagation time depends on frequencies because the refraction index at each layer differs from each frequency according to the dispersion in the ionosphere. The propagation time at 30 MHz is 4 μ s longer than at 100 MHz, for instance. The time lag of the X mode propagation from the O mode is several tens ns. Figure 13 represents the propagation time difference between two modes at incident angles of 30° and 70°. It can be seen that the smaller incident angle corresponds to the longer time separation of the

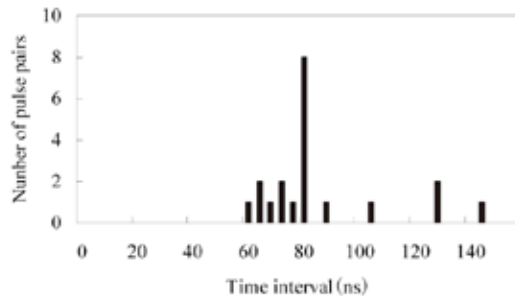


Figure 14. Frequency distribution of time intervals between observed pulse pairs.

pulse pair from Fig. 13. Figure 14 shows the frequency distribution of the time interval observed by Maido-1. The peak value of 80 ns and the distribution agree with the simulated time difference in Fig. 13, which is equal to the time interval of pulse pair. It can be concluded that the observed pulse pairs are caused by the mode splitting.

5. Direction-of-arrival estimation considering the ionospheric propagation

The group delay in broadband EM waveform received at satellite after propagation through the dispersive ionosphere depends on frequency as described above. According to the observations at the same satellite location and the same ionospheric condition, in other words, the difference of arrival time between frequencies becomes large in correlated with the distance from the EM radiation source. The farther source has the larger incident angle and the longer propagation path, resulting in the larger delay. The estimation of the direction-of-arrival (DOA) from the observed waveform is attempted in this chapter. The incident angle to the nadir source is defined 0° in this paper.

Figure 15 shows the spectrogram of the waveform recorded at 2323:25h (UTC) on February 12, 2009 over Africa. Figure 15 is drawn by the vertically arranged Fourier spectra with sliding time window in each sampling, i.e. the time evolution of the Fourier spectra. The curve of high spectral intensity is noticeable as lined in white in Fig. 15. The gray line in the figure indicates the time series of the peak frequencies which are calculated to the nadir source using the model in Section 3.3. The charge density of the time and the location is input from the IRI model. The dispersion curve is calculated for every one degree in the incident angle with reference to the nadir source, and the angle providing the most correlated curve with the observed curve (white line in Fig. 15) is considered as the estimated DOA. The DOA is estimated as 49° in this case. Lightning

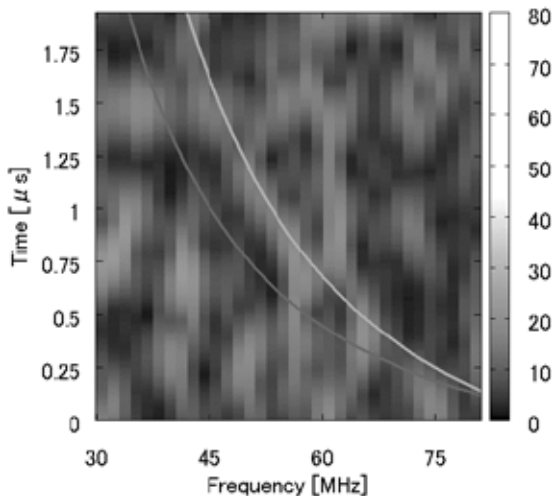


Figure 15. Spectrogram of the VHF waveform recorded at 2323:25 (UTC) on February 12, 2009.

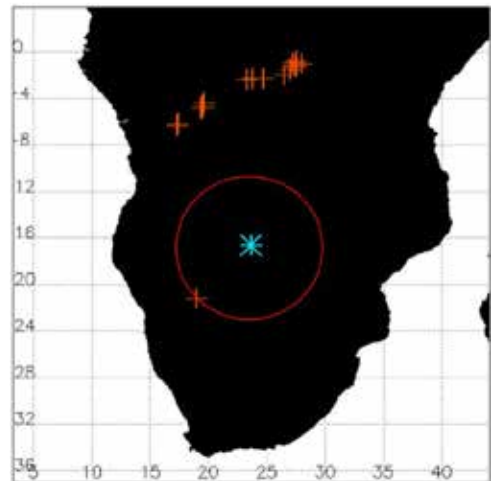


Figure 16. Lightning locations estimated by Maido-1 and WLLN.

discharges located by WWLLN at the same time are mapped in Fig. 16. Crosses (+) and asterisk (*) indicate the locations of the lightning by WWLLN and the Mido-1 where the VHF sensor records the waveform, respectively. The estimated DOA is also drawn in Fig. 16 as a circle. The circle is the intersection of the Earth’s surface and the conical surface with the tip at the location of Maido-1 and a conical angle of 49° . The DOA estimation is in very good agreement with the WWLLN observations. The results for other observations are reported in Kikuchi *et al.* (2013).

6. Concluding remarks

A group of SMEs and universities in Kansai region developed a small satellite with technology transfer from JAXA MicroLabSat. The developed satellite is a spin-stabilized microsatellite with the weight of 57 kg with the concept of simple and low cost. The satellite was launched and named as Maido-1 on January 23, 2009, and then operated for nine months. The authors conducted the main scientific mission of lightning observations to examine the feasibility of the space-borne DITF by receiving VHF lightning impulses in space. The VHF sensor on Maido-1 conducted 158 lightning observations and recorded about 15,000 VHF EM waveforms around the world without any mechanical problems. The instrument manufactured by many COTS parts were functionally verified.

The recorded EM waveforms have a regional dependency. The weak signal at non-active lightning area confirms that the EM background at the orbit is acceptable for VHF observations. Vary of the FWHM of recoded waveforms are considered to reflect the DOA because of the dispersion in the ionosphere. It is replicated by the numerical simulation for the ionosphere model with spherical layers. With an expansion of the simulation model, the cause of the observed pulse pair is concluded as the mode splitting in the ionospheric propagation. The adequacy of the designed sensitivity is validated as well. Furthermore, we proposed the estimation considering the ionospheric propagation and demonstrated its effectiveness.

The achievements of the VHF sensor on Maido-1 satellite were followed by the Global Lightning and Sprite Measurement (GLIMS) mission at the Exposed Facility of Japanese Experiment Module (JEM-EF) of the International Space Station (ISS). GLIMS mission has achieved the world's first lightning observations by means of space-borne VHF interferometry (Sato *et al.* 2015; Kikuchi *et al.* 2016; Morimoto *et al.* 2016).

Acknowledgement. The development of Maido-1 was funded by the New Energy and Industrial Technology Development Organization (NEDO) as a key technology research promotion program. Maido-1 was launched as Micro Piggyback Satellite Launches of JAXA. A lot of crucial support and helps were provided by the Space Technology Demonstration Research Center of JAXA throughout the project. WWLLN data were provided by R. Holzworth (University Washington, USA) with collaboration among over 50 universities and institutions. IRI and IGRF model data were obtained from the Community Coordinated Modeling Center, NASA. The authors cordially acknowledge

them as well as the engineers of companies that contributed towards development, especially Dainichi Denshi Co., Ltd. and Japan Communication Equipment Co., Ltd.

References

- Boccippio DJ, Goodman SJ, Heckman S 321 (2000) Regional difference in tropical lightning distributions, *J. Applied Meteorology*, vol. 39, pp. 2231-224
- Christian HJ, Blakeslee RJ, Boccippio DJ, Boeck WL, Buechler DE, Driscoll KT, Goodman SJ, Hall JM, Koshak WJ, Mach DM, Stewart MF (2003) Global frequency and distribution of lightning as observed from space by the Optical Transient Detector, *J. Geophysical Research*, vol. 108, no. D1, 4005, doi:10.1029/2002JD002347
- IGRF database (2009) Virtual Ionosphere, The Community Coordinated Modeling Center, NASA. http://ccmc.gsfc.nasa.gov/modelweb/models/igrf_vitmo.php
- IRI database (2007) Virtual Ionosphere, The Community Coordinated Modeling Center, NASA. http://ccmc.gsfc.nasa.gov/modelweb/models/iri_vitmo.php
- Kato M, Takayama S, Nakamura Y, Yoshihara Y, Hashimoto H, (2005) Road map of small satellites in JAXA. In: 56th International Astronautical Congress (IAC), IAC-05.B5.6.B.01, Fukuoka, Japan
- Kikuchi H, Tanaka R, Morimoto T, Ushio T, Kawasaki Z, Aoki T, Hashimoto H (2010a) Observations of lightning discharges by Maido-1 satellite and radio propagation simulations, In: Workshop on Technical Committee on Electromagnetic Compatibility, EMC-10-25 (in Japanese)
- Kikuchi H, Tanaka R, Yoshida S, Morimoto T, Ushio T, Kawasaki Z (2010b) Observations of lightning discharges from space and frequency characteristics through the ionosphere, In: Annual Meeting on Electromagnetic Theory, EMT-10-105 (in Japanese)
- Kikuchi H, Yoshida S, Morimoto T, Ushio T, Kawasaki Z, (2011) Satellite observations for lightning discharges and analysis of VHF electromagnetic waveforms, *The Institute of Electrical Engineering of Japan (IEEJ) Trans. on Fundamentals and Materials*, vol. 131, no.9, pp.705-710
- Kikuchi H, Yoshida S, Morimoto T, Ushio T, Kawasaki Z, (2013) VHF radio wave observations by Maido-1 satellite and evaluation of its relationship with lightning discharges, *The Institute of Electronics, Information and Communications Engineering Trans. on Communications*, vol. E96-B, no.3, pp.880-886
- Kikuchi H, Morimoto T, Sato M, Ushio T, Kikuchi M, Yamazaki A, Suzuki M, Ishida R, Sakamoto Y, Kawasaki Z (2016) Direction-of-arrival estimation of VHF signals recorded on the International Space Station and simultaneous of optical lighting, *The Institute of Electrical and Electronics Engineers (IEEE) Trans. on Geoscience and Remote sensing*, vol. 54, no.7, pp.3868-3877
- Mardiana R, Kawasaki Z, Morimoto T (2000) Three-dimensional lightning observations of cloud-to-ground flashes using broadband interferometers, *J. Atmospheric and Solar-Terrestrial Physics*, vol. 64, no.1, pp. 91-103

- Morimoto T, Hirata A, Kawasaki Z, Ushio T, Matsumoto A, Lee JH (2004) An operational VHF broadband digital interferometer for lightning monitoring, *IEEJ Trans. on Fundamentals and Materials*, vol. 124, no.12, pp.1232-1238
- Morimoto T, Kikuchi H, Sato M, Suzuki M, Yamazaki A, Ushio T (2011) VHF lightning observations on JEM-GLIMS mission – Gradual approach to realizing space-borne VHF broadband digital interferometer -, *IEEJ Trans. on Fundamentals and Materials*, vol. 131, no. 12, pp. 977-982
- Morimoto T, Kikuchi H, Sato M, Ushio T, Yamazaki A, Suzuki M, Ishida R, Sakamoto Y, Yoshida K, Hobara Y, Sano T, Abe T, Kawasaki ZI (2016) An overview of VHF lightning observations by digital interferometry from ISS / JEM-GLIMS, *Earth, Planets and Space*, vol.68, article 145, doi:10.1186/s40623-016-0522-1
- Nakamura, Y, A. Noda, H. Hashimoto, S. Kimura, S. Nishida, S. Nakasuka (2003) *icrolabsat*. In: 54th IAC, IAC-03.IAA.11.1.08, Bremen, Germany
- Nakamura, Y, H. Hashimoto (2004) Technology transfer program of *Microlabsat*. In: 56th IAC, IAC-05.B5.6.B.08, Fukuoka, Japan
- Nakamura, Y., H. Hashimoto (2005) *SOHLA-1*, a low cost satellite development with technology transfer program of JAXA. In: 4th Symposium: Small Satellites Systems and Services, RSA SP-571, La Rochelle, France
- Ohtsubo, Y. Nakamura, N. Takahashi, T. Nakamura, A. Noda, H. Hashimoto (2003) Overview and status of *MicroLabsat*. In: Center Conference and FedSat Workshop Program, p.14, Adelaide, Australia
- Okubo, H., H. Azuma (2006) Activities of Small Spacecraft Systems Research Center and on-going projects. In: 25th International Symposium on Space Technology and Science and 19th International Symposium on Space Flight Dynamics, 2006-o-3-06v, Ishikawa, Japan
- Okubo, H., M. Chiba, H. Azuma (2009) Development and operation of microsatellite “*SOHLA-1 (Maido-1)*”. In: 60th IAC, IAC-09.B4.3.8, Daejeon, Korea
- Sato M, Ushio T, Morimoto T, Kikuchi M, Kikuchi H, Adachi T, Suzuki M, Yamazaki A, Takahashi Y, Inan U, Linscott I, Ishida R, Sakamoto Y, Yoshida K, Hobara Y, Sano T, Abe T, Nakamura M, Oda H, Kawasaki ZI (2015) Overview and early results of the Global Lightning and Sprite Measurements mission, *J. Geophysical Research Atmosphere*, 120, doi:10.1002/2014JD022428
- Sen HK, Wyller AA (1960) On the generalization of the Appleton-Hartree Magnetoionic Formulas, *J. Geophysical Research*, vol. 65, no.12, pp.3931-3950
- Taniguchi T, Hirata A, Morimoto T, Kawasaki Z (2006) Propagation characteristics of wideband electromagnetic wave in the ionosphere, *IEEJ Trans. on Fundamentals and Materials*, vol. 126, no. 11, pp. 1173-1176 (in Japanese)
- Tierney HE, Jacobson AR, Roussel-Dupre R, Beasley WH (2002) Trans ionospheric pulse pairs originating in maritime, continental and coastal thunderstorms: Pulse energy ratios, *Radio Science*, vol. 37, no.3, 1039, doi:10.1029/2001RS002506

(Received August 31 2016, 2015; revised January 31 2017;
accepted January 31 2017)

